

Density-ratio-invariant mean-species profile of classical Rayleigh-Taylor mixing

Yu-cang Ruan¹, You-sheng Zhang^{2,3,*}, Bao-lin Tian^{2,3,†} and Xin-ting Zhang¹

¹*Beihang University, Sino-French Engineer School, Beijing 100191, China*

²*Institute of Applied Physics and Computational Mathematics, Beijing 100094, China*

³*Center for Applied Physics and Technology, HEDPS, and College of Engineering, Peking University, Beijing 100871, China*



(Received 23 September 2019; accepted 14 April 2020; published 8 May 2020)

Accurately predicting profiles of mean-mass fraction \bar{Y} and mean-molar/volume fraction $\bar{\Phi}$ (equivalent to renormalized mean density $\bar{\rho}$) of turbulent mixing induced by Rayleigh-Taylor instability at different density ratio R is of fundamental importance for many natural phenomena and engineering applications but has not been quantified yet. Based on asymptotic analysis, we give an R -invariant hybrid profiles $C(X) \equiv F\bar{Y} + (1-F)\bar{\Phi}$ with $A \equiv (R-1)/(R+1)$ and $F \equiv (1+A)(1-X)/2$ and derive the analytical expression of $C(X)$, where $X \in [0, 1]$ is a mixing-width-rescaled dimensionless coordinate. The invariance are validated by both experiments and simulations. Consequently, combining the R invariance of $C(X)$ and the relation of $\bar{\Phi} = \bar{Y}/[\bar{Y} + (1-\bar{Y})R]$ derived from definitions, the mean profiles of density, mass fraction, and molar/volume fraction at different density ratios are accurately predicted.

DOI: [10.1103/PhysRevFluids.5.054501](https://doi.org/10.1103/PhysRevFluids.5.054501)

I. INTRODUCTION

When a heavy fluid of density ρ_h located at $x < 0$ region is accelerated by a light fluid of density ρ_l located at an $x > 0$ region, any irregular perturbation presented at the material interface would develop and transition quickly to turbulence. The heavy (light) fluid penetrates into light (heavy) fluid to form a spikes (bubbles) mixing zone [1,2]. The spikes mixing zone edge $h_s > 0$ is generally defined as the location with the mean-molar fraction of heavy fluid $\bar{\Phi} = \psi$. The bubbles mixing zone edge $h_b < 0$ is generally defined as the location with the mean-molar fraction of heavy fluid $\bar{\Phi} = 1 - \psi$. ψ is the edge criterion, which can be 0.01 [3], 0.05 [4], and other values [1,5] according to different researchers. This process is called turbulent mixing induced by Rayleigh-Taylor (RT) instability [6,7] and occurs ubiquitously [8] in systems ranging from a micro- [9] to an astronomical scale [1]. For classical RT mixing with constant acceleration of g , the mixing evolution is determined [10] only by the density ratio $R \equiv \rho_h/\rho_l$ or equivalently the Atwood number $A \equiv (R-1)/(R+1) \in [0, 1]$.

The RT mixing process plays a crucial role for many natural phenomena (e.g., supernova explosions [11]) and engineering applications [1,12] especially in all known forms of fusion [3], whether the confinement is magnetic [13], inertial [14,15], or gravitational [16]. In these problems, due to the sensitivity of thermonuclear reactions to the flow fields, the accurate prediction of the total mixed mass [17,18] as well as the mean-density profile $\bar{\rho}$ [1,19] plays a vital role in predicting fusion ignition and nuclear energy yields [19]. The mixed mass, for example, can be obtained by

*zhang_yousheng@iapcm.ac.cn

†tian_baolin@iapcm.ac.cn

integrating the profiles of mean density $\bar{\rho}$ and mean mass fraction of heavy fluid \bar{Y} over the mixing zone [18], whose width of $h \equiv h_s - h_b$ evolving with time of t has been well formulated [20]. As for $\bar{\rho}$, its dimensionless renormalized profile of $(\bar{\rho} - \rho_l)/(\rho_h - \rho_l)$ is equivalent [21] to the mean-molar/volume fraction $\bar{\Phi}$. Moreover, $\bar{\Phi}$ has the intrinsic relation with \bar{Y} as

$$\bar{\Phi} = \bar{Y}/[\bar{Y} + (1 - \bar{Y})R], \quad (1)$$

which is derived from their definitions (neglecting the high-order fluctuations) [10]. Consequently, the prediction of the mixed mass and density profile is turned to predict the profile of either $\bar{\Phi}$ or \bar{Y} . Up to now, only a few experimental [22–24] and numerical [10,25] profiles of $\bar{\Phi}$ and \bar{Y} have been reported at specific density ratios. These data show that their profiles change dramatically with the density ratio (see Fig. 1), resulting in difficulty in quantifying these profiles.

Up to now, no theory on the profile of either $\bar{\Phi}$ or \bar{Y} has yet been established in literature. In this paper, we show that the mean-mass fraction and mean-molar fraction hybrid profile (i.e., the left side of the following equation) is independent of density ratio:

$$F\bar{Y} + (1 - F)\bar{\Phi} = C, \quad (2)$$

where $F \equiv (1 + A)(1 - X)/2$ is a weighted function of mean-mass fraction, $X \equiv (x - h_b)/(h_s - h_b) \in [0, 1]$ is a mixing-width-rescaled dimensionless coordinate, and $C(X)$ denotes the R -invariant profile that was derived analytically. This R invariance was determined through asymptotic analysis and theoretical derivation, and validated by both experiments and simulations. By combining Eqs. (1) and (2), the profiles of \bar{Y} , $\bar{\Phi}$, and $\bar{\rho}$ at different density ratios ($R > 1$) can be given analytically as

$$\bar{Y} = \frac{F + C + (R - 1)^{-1} - \sqrt{\Delta}}{2F}, \quad (3)$$

$$\bar{\Phi} = \frac{F + C + (R - 1)^{-1} - \sqrt{\Delta}}{(R + 1)F + (1 - R)C - 1 + (R - 1)\sqrt{\Delta}}, \quad (4)$$

and accurately predicted (see Fig. 2) with $\Delta = [F + C + (R - 1)^{-1}]^2 - 4CRF(R - 1)^{-1}$. Thus, this is of great significance to science and other applications.

II. THEORY AND DERIVATIONS

We first present the invariance from analyzing the variation of \bar{Y} and $\bar{\Phi}$ with density ratio as shown in Figs. 1(a) and 1(b), respectively. In Fig. 1 the growth of the mixing zone was implicitly taken into consideration through the renormalization of the space coordinate x with the mixing width $h_{b,s}$, i.e., $X \equiv (x - h_b)/(h_s - h_b)$. Under this renormalized spatial coordinate X , due to the self-similar evolution of fully developed turbulence, the plot of profiles of $\bar{Y}(X, A)$ and $\bar{\Phi}(X, A)$ against the dimensionless abscissa X at different time would collapse together. Based on Fig. 1 or Eq. (1), we can make the following two thought experiments: (1) when $A \rightarrow 0$ ($R \rightarrow 1$), \bar{Y} and $\bar{\Phi}$ are equivalent, and (2) when $A \rightarrow 1$ ($R \rightarrow \infty$), profiles of \bar{Y} and $\bar{\Phi}$ form a hysteresis-like loop with $\bar{Y}(1, 1) \rightarrow 1$, $\bar{\Phi}(1, 1) \rightarrow 0$. Inspired by these thought experiments, we defined a transformation as follows:

$$\bar{Y}F + \bar{\Phi}G = C, \quad (5)$$

where, in principle, \bar{Y} , $\bar{\Phi}$, F , G , and C are functions of (X, A) . For simplicity, we did not express this dependence explicitly. We want to find the appropriate weighted functions F and G such that C would be a profile independent on A . Moreover, the first thought experiment implied that the simplest universal profile could be the profile of \bar{Y} at $A \rightarrow 0$, i.e., $C(X) \equiv \bar{Y}(X, 0^+)$.

We proposed a possible proposition for F and G based on the two thought experiments described above. First, by substituting the deduction of the first thought experiment into the proposed

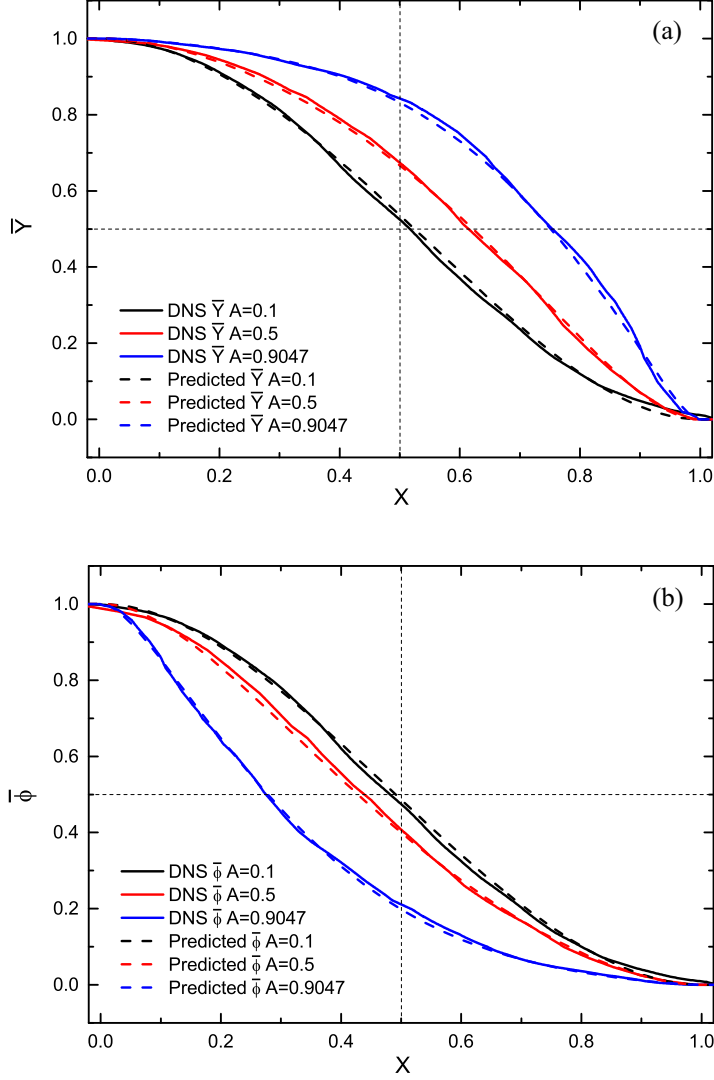


FIG. 1. Theoretical and numerical variation of \bar{Y} in (a) and $\bar{\Phi}$ in (b) vs X at different R . The three curves located on the upper right and lower left are \bar{Y} and $\bar{\Phi}$, respectively. The solid and dashed lines denote, respectively, the profiles of the numerical simulations and theoretical predictions by combining Eqs. (1) and (2). The black, red, and green lines correspond to the cases with density ratio $R = 11:9$, $3:1$, and $20:1$ ($A = 0.1$, 0.5 , and 0.9), respectively.

transformation equation (5), the following equation was derived:

$$F(X, A) + G(X, A) = 1, \quad (6)$$

where $A \rightarrow 0$. Similarly, by substituting the deduction of the second thought experiment into Eq. (5), we can infer that $F(1, 1) = 0$. The supposition of the inferences of two thought experiments at the same given time for F becomes $F = (1 + A)(1 - X)/2$ (one possible proposition). G was further obtained by supposing that Eq. (6) is applicable for an arbitrary density ratio. A substitution of the two suppositions into Eq. (5) gave Eq. (2).

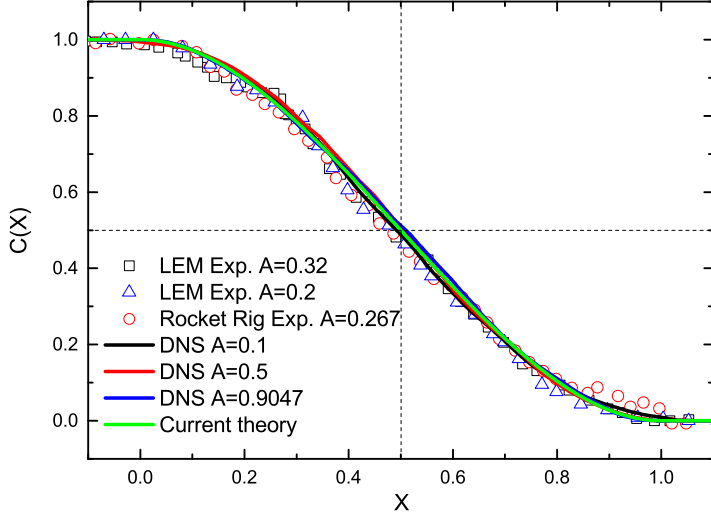


FIG. 2. Theoretical, numerical, and experimental variations of density-ratio-invariant profile C vs X at different R . The circle and triangle symbol denote the experimental results conducted in a linear-electric-motor at $R = 1.96:1$ ($A = 0.32$) and $R = 1.5:1$ ($A = 0.2$) [23,24], respectively. The square symbol denotes the experimental results conducted with Rocket Rig at $1.73:1$ ($A = 0.267$) [22]. The black, red, and blue lines denote the numerical profiles with density ratio $R = 11:9$, $3:1$, and $20:1$ ($A = 0.1$, 0.5 , and 0.9), respectively. The green line denotes the R -invariant universal profile predicted by analytical theory, i.e., Eq. (10).

We tested the proposed R invariance of Eq. (2) through reliable numerical simulations for classic RT mixing at density ratios of $R = 11:9$, $3:1$, and $20:1$ ($A = 0.1$, 0.5 , and 0.9) using the Code of Finite Difference for Compressible Fluid Dynamics (CFD²) developed by You-sheng Zhang *et al.* [26]. The Navier-Stokes equation coupled with the state of ideal gas equation were used to give an approximate description of the mixing of two incompressible fluids. The problem configurations [10,25], numerical methods [10], and mesh resolution [10] were the same as those of Refs. [10,25]. The reliability of the simulations using the above settings and methods were fully demonstrated in literature [10] and thus are not given in this paper. The statistical profiles were obtained using the following procedures: (1) after the turbulent mixing entering the self-similar stage, an average of the instantaneous quantify $f(x, y, z, t)$ in the yz plane (perpendicular to the mixing direction x) was conducted to obtain spatial mean $\bar{f}(x, t)$; (2) to obtain a very smooth profile, after mapping the $\bar{f}(x, t)$ in the X space to obtain $\bar{f}(X, t)$, the $\bar{f}(X, t)$ is further averaged along the time direction t to obtain the final profile $\bar{f}(X)$.

The profiles of $C(X)$ computed from current simulations and the well-known RT mixing experiments [22,23,25] are plotted in Fig. 2. The results shows that all profiles collapsed at different density ratios, hence, validating the R invariance of the hybrid species profile described by Eq. (2). Therefore, the remaining task is to derive the analytical expression of $C(X)$. Considering the R invariance of profile $C(X)$, the theoretical derivation is equivalent to solving the analytical profile of \bar{Y} at any A . Obviously, the simplest case is the profile at $A \rightarrow 0^+$, i.e., $C(X) \equiv \bar{Y}(X, 0^+)$, whose analytical expression is obtained in this paper by jointly solving the mass fraction equation and momentum equation at $A \rightarrow 0^+$, following the same methodology and approach employed by Boffetta [27] for the temperature profile of Rayleigh-Taylor mixing.

First, by averaging the mass fraction equation, $Y_t + \nabla \cdot (\mathbf{u}Y) = \nabla \cdot (D_m \nabla Y)$ over the yz plane (assumed periodic), we can derive the corresponding averaged equation as follows:

$$\bar{Y}_t + (\bar{u}\bar{Y})_x = (D_m \bar{Y}_x)_x, \quad (7)$$

where \mathbf{u} is velocity and D_m is molecular diffusivity of the mass fraction. The mass flux term $\overline{u\bar{Y}}$ makes Eq. (7) an unclosed form expression. Using a common approach to turbulence [27], in terms of the eddy diffusivity hypothesis of $\overline{u\bar{Y}} = -D_t \bar{Y}_x$ we were able to transform Eq. (5) into the following equation:

$$\bar{Y}_t = (D\bar{Y}_x)_x, \quad (8)$$

where $D \equiv D_m + D_t$ and D_t are the total and turbulent diffusivity of the mass fraction, respectively. However, in fully developed turbulence, D_t is generally much larger than D_m and is frequently neglected. \bar{Y} from Eq. (8) can be determined using only a known D . In our study, we assumed the evolution of D through the following considerations: (1) in physics, the diffusivity of \bar{Y} is dependent on \bar{Y} , and, more specifically, it is proportional to the spatial gradient of \bar{Y} , i.e. $D \propto \bar{Y}_x$; (2) the assumed relationship should have the same dimensions as that of $D \sim [L]^2[t]^{-1}$, and in RT mixing the most important and characteristic mixing width h has a length dimension L . Therefore, we have $D \propto h^3 t^{-1} \bar{Y}_x$.

Second, we further evaluate the evolution of mixing width h from the momentum equation $\mathbf{u}_t + \mathbf{u} \cdot \nabla \mathbf{u} = \nu \Delta \mathbf{u} - \nabla p / \rho + \mathbf{g}$, where ν is kinetic viscosity and p is pressure. Using Eq. (1), the momentum equation can be rearranged to give

$$\mathbf{u}_t + \mathbf{u} \cdot \nabla \mathbf{u} = \nu \Delta \mathbf{u} - \nabla P / \rho + 2AY\mathbf{g}, \quad (9)$$

where $P \equiv p - \rho_l \mathbf{g} \cdot \mathbf{x}$ should be regarded as a general pressure. Equation (9) implies that the global potential energy $E_p \equiv \langle 2AYgx \rangle$, where $\langle \rangle$ represents the integral over the mixing domain. Next, the principle of energy transformation yields $-\dot{E}_p = \dot{E}_k + \epsilon_v$, where $\dot{E}_p = \langle 2AYgu \rangle$, $E_k \equiv \langle u^2/2 \rangle$ is global kinetic energy with $\dot{E}_k = \langle u\dot{u} \rangle$, and ϵ_v is the viscous dissipation rate. Consequently, integrating the order relation of $\dot{E}_p \sim \dot{E}_k$ over time immediately gives $h \propto Agt^2$, i.e., the well-known quadratic law [1].

Collecting the above results, we thus assumed $D = c_1 h^3 t^{-1} \bar{Y}_x$, where c_1 is an undetermined dimensionless constant. Now Eq. (8) can be integrated analytically. In mathematics, this equation is a specific example of a nonlinear diffusion equation with an analytical solution that has been discussed in the literature [28]. We introduced a middle variable, $\eta \equiv x/h$, to aid in showing the process of solving Eq. (8). We used the symmetry of $h_b = -h_s$ and the quadratic law of $h \sim Agt^2$ obtained above to derive $\eta = X - 1/2$, $\eta_t = -2\eta/t$, $\eta_x = -1/h$ and replaced the partial derivation $f_{x/t}$ in Eq. (8) with the chain rule $f_{x/t} = f_\eta \eta_{x/t}$; this gave $\bar{Y}_{\eta\eta} = -\eta/c_1$, whose solution is

$$C(X) = \begin{cases} 1, & X < X_l^e \\ \frac{(X-1/2)^3}{-6c_1} + c_2(X-1/2) + c_3, & \text{others} \\ 0, & X > X_r^e \end{cases}, \quad (10)$$

where X_l^e and X_r^e denote, respectively, the point corresponding to the left extreme point of $C_X = 0$ ($X \leq 0$) and the right extreme point of $C_X = 0$ ($X \geq 1$), and $c_{1,2,3}$ are constants. The values of constants $c_{1,2,3}$ are determined using the following requirements: (1) the definitions of h_b and h_s require $C|_{X=0} = 1 - \psi$ and $C|_{X=1} = \psi$ and (2) the asymptotic variation of physical C requires that $C(X_l^e) = 1$ (or equivalently $C(X_r^e) = 0$). Obviously, the values of $c_{1,2,3}$, as well as X_l^e and X_r^e , are essentially determined by the value of ψ , i.e., the truncated value of mixing width. As mentioned at the beginning, however, different values of ψ have been used in different literature. To avoid the artificialness introduced by different definitions, $\psi = 0$ is used in this paper. Under this condition, we have $c_1 = -1/12$, $c_2 = -3/2$, $c_3 = 1/2$, $X_l^e = 0$, and $X_r^e = 1$.

III. RESULTS AND DISCUSSIONS

In Fig. 2 we plotted the universal profile $C(X)$ of Eq. (10) using simulations and experiment results. In this figure, in terms of asymptotic behavior, the values beyond the two extrema corresponding to $C_X = 0$ is imposed either 0 or 1 [28]. This figure shows that the theoretical profiles

coincide with the numerical simulations and experimental results, validating the R invariance of the mean-species profile we found in this study.

The R invariance may have many applications. One direct application is to predict the mean profiles of volume fractions, mass fractions, molar fractions, and density at different density ratios. The predictions can be achieved by jointly solving Eqs. (1), (2), and (10). In Fig. 1 the predicted profiles of \bar{Y} and $\bar{\Phi}$ at different density ratios are compared with those of reliable numerical simulations. From this figure, we can see that the predictions almost collapse entirely with the simulations, highlighting the significance of the R invariance we found in this paper. Other applications include the predictions of mixed mass [18], molecular mixing degree, and mixed width (the last two will be published elsewhere).

We find some discussion in order. The R invariance shown in Eq. (2) was established on the nondimensional spatial coordinate X , which was renormalized by $h_{b,s}$. Therefore, an accurate definition of the position of $h_{b,s}$ is important for the R invariance. Unfortunately, as mentioned in Sec. I, up to now there has not been a unified definition of the $h_{b,s}$. Moreover, in practice it is very difficult to obtain a smooth $\bar{\Phi}$ profile to accurately define the position of $h_{b,s}$, especially in experiments. To avoid the artificialness introduced by these factors, the ideal truncation of $\bar{\Phi} = 0$ is used in this paper. However, it is worth pointing out that $\bar{\Phi}$ changes very slowly near this value. A very slight variation of $\bar{\Phi}$ near $\bar{\Phi} = 0$ generally corresponds to an observable variation of x . Therefore, if a small deviation in determining the position of $h_{b,s}$ occurs, a shift in X , and thus the R invariance, can be observed. Fortunately, this deviation mainly shifts the universal profile but not change its shape. Therefore, as another possible application, one can use this property and the R invariance to accurately define the position of $h_{b,s}$, especially for the experiments.

In addition, it is worth pointing out that in this paper the simulations used to validate this R invariance theory is perturbed with random short-wave perturbations, as frequently used in literature [25]. As we known, however, the evolution of RT mixing strongly depends on initial perturbations if it includes long wavelength [10,29,30]. For this kind of mixing, the correctness and effectiveness of the above theories need to be reevaluated and even modified. However, this is beyond the scope of this paper, and we leave this issue to the future. Finally, we mention that the method, idea, and logic presented in this paper may also work for Richtmyer-Meshkov mixing [31,32].

ACKNOWLEDGMENT

We acknowledge financial support from the National Natural Science Foundation of China (NSFC) under Grants No. 11972093, No. 91852207, and No. U1630138.

-
- [1] Y. Zhou, Rayleigh-Taylor and Richtmyer-Meshkov instability induced flow, turbulence, and mixing. II, *Phys. Rep.* **723–725**, 1 (2017).
 - [2] Z.-R. Zhou, Y.-S. Zhang, and B.-L. Tian, Dynamic evolution of Rayleigh-Taylor bubbles from sinusoidal, W-shaped, and random perturbations, *Phys. Rev. E* **97**, 033108 (2018).
 - [3] A. W. Cook and W. H. Cabot, Reynolds number effects on Rayleigh-Taylor instability with possible implications for type Ia supernovae, *Nat. Phys.* **2**, 562 (2006).
 - [4] M. S. Roberts and J. W. Jacobs, The effects of forced small-wavelength, finite-bandwidth initial perturbations and miscibility on the turbulent Rayleigh-Taylor instability, *J. Fluid Mech.* **787**, 50 (2016).
 - [5] Y. Zhou, Rayleigh-Taylor and Richtmyer-Meshkov instability induced flow, turbulence, and mixing. I, *Phys. Rep.* **720–722**, 1 (2017).
 - [6] L. Rayleigh, Investigation of the character of the equilibrium of an incompressible heavy fluid of variable density, *Proc. Lond. Math. Soc.* **s1–14**, 170 (1882).
 - [7] G. Taylor, The instability of liquid surfaces when accelerated in a direction perpendicular to their planes. I, *Proc. R. Soc. A* **201**, 192 (1950).

- [8] D. Livescu, Numerical simulations of two-fluid turbulent mixing at large density ratios and applications to the Rayleigh-Taylor instability, *Philos. Trans. R. Soc. Lond. A* **371**, 20120185 (2013).
- [9] M. Versluis, B. Schmitz, A. von der Heydt, and D. Lohse, How snapping shrimp snap: Through cavitating bubbles, *Science* **289**, 2114 (2000).
- [10] D. L. Youngs, The density ratio dependence of self-similar Rayleigh-Taylor mixing, *Philos. Trans. R. Soc. Lond. A* **371**, 20120173 (2013).
- [11] A. Burrows, Supernova explosions in the universe, *Nature (London)* **403**, 727 (2000).
- [12] P. N. Rowe, B. A. Partridge, E. Lyall, and G. M. Ardran, Bubbles in fluidized beds, *Nature (London)* **195**, 278 (1962).
- [13] G. Bateman, *MHD Instabilities* (MIT Press, Cambridge, MA, 1978).
- [14] R. D. Petrasso, Rayleigh's challenge endures, *Nature (London)* **367**, 217 (1994).
- [15] R. P. Taleyarkhan, C. D. West, J. S. Cho, R. T. Lahey, R. I. Nigmatulin, and R. C. Block, Evidence for nuclear emissions during acoustic cavitation, *Science* **295**, 1868 (2002).
- [16] M. Zingale, S. E. Woosley, C. A. Rendleman, M. S. Day, and J. B. Bell, Three-dimensional numerical simulations of Rayleigh-Taylor unstable flames in type Ia supernovae, *Astrophys. J.* **632**, 1021 (2005).
- [17] Y. Zhou, W. H. Cabot, and B. Thornber, Asymptotic behavior of the mixed mass in Rayleigh-Taylor and Richtmyer-Meshkov instability induced flows, *Phys. Plasmas* **23**, 052712 (2016).
- [18] Y. S. Zhang, Y. C. Ruan, H. S. Xie, and B. L. Tian, Mixed mass of classical Rayleigh-Taylor mixing at arbitrary density ratios, *Phys. Fluids* **32**, 011702 (2020).
- [19] V. A. Thomas and R. J. Kares, Drive Asymmetry and the Origin of Turbulence in an ICF Implosion, *Phys. Rev. Lett.* **109**, 075004 (2012).
- [20] Y.-s. Zhang, Z.-w. He, F.-j. Gao, X.-l. Li, and B.-l. Tian, Evolution of mixing width induced by general Rayleigh-Taylor instability, *Phys. Rev. E* **93**, 063102 (2016).
- [21] P. F. Linden, J. M. Redondo, and D. L. Youngs, Molecular mixing in Rayleigh-Taylor instability, *J. Fluid Mech.* **265**, 97 (1994).
- [22] D. L. Youngs, Modelling turbulent mixing by Rayleigh-Taylor instability, *Physica D* **37**, 270 (1989).
- [23] G. Dimonte and R. Tipton, *K-L* turbulence model for the self-similar growth of the Rayleigh-Taylor and Richtmyer-Meshkov instabilities, *Phys. Fluids* **18**, 85101 (2006).
- [24] G. Dimonte and M. Schneider, Density ratio dependence of Rayleigh-Taylor mixing for sustained and impulsive acceleration histories, *Phys. Fluids* **12**, 304 (2000).
- [25] G. Dimonte, D. L. Youngs, A. Dimits, S. Weber, M. Marinak, S. Wunsch, C. Garasi, A. Robinson, M. J. Andrews, P. Ramaprabhu *et al.*, A comparative study of the turbulent Rayleigh-Taylor instability using high-resolution three-dimensional numerical simulations: The Alpha-Group collaboration, *Phys. Fluids* **16**, 1668 (2004).
- [26] H.-f. Li, Z.-w. He, Y.-s. Zhang, and B.-l. Tian, On the role of rarefaction/compression waves in Richtmyer-Meshkov instability with reshock, *Phys. Fluids* **31**, 54102 (2019).
- [27] G. Boffetta, F. De Lillo, and S. Musacchio, Nonlinear Diffusion Model for Rayleigh-Taylor Mixing, *Phys. Rev. Lett.* **104**, 034505 (2010).
- [28] R. E. Pattle, Diffusion from an instantaneous point source with a concentration-dependent coefficient, *Q. J. Mech. Appl. Math.* **12**, 407 (1959).
- [29] G. Dimonte, Dependence of turbulent Rayleigh-Taylor instability on initial perturbations, *Phys. Rev. E* **69**, 056305 (2004).
- [30] P. Ramaprabhu, G. Dimonte, and M. J. Andrews, A numerical study of the influence of initial perturbations on the turbulent Rayleigh-Taylor instability, *J. Fluid Mech.* **536**, 285 (2005).
- [31] F.-j. Gao, Z.-w. He, Y.-s. Zhang, L. Li, and B.-l. Tian, The characteristic of turbulent mixing at late stage of the Richtmyer-Meshkov instability, *AIP Adv.* **7**, 075020 (2017).
- [32] F.-j. Gao, Y.-s. Zhang, Z.-w. He, and B.-l. Tian, Formula for growth rate of mixing width applied to Richtmyer-Meshkov instability, *Phys. Fluids* **28**, 114101 (2016).